

## Wintertime Winds in and around the Ulaanbaatar Metropolitan Area in the Presence of a Temperature Inversion

Gantuya Ganbat<sup>1,2</sup> and Jong-Jin Baik<sup>1</sup>

<sup>1</sup>School of Earth and Environmental Sciences, Seoul National University, Seoul, Korea

<sup>2</sup>Information and Research Institute of Meteorology, Hydrology and Environment, Ulaanbaatar, Mongolia

(Manuscript received 18 August 2015; accepted 1 March 2016)  
© The Korean Meteorological Society and Springer 2016

**Abstract:** Temperature inversions are frequently observed in mountainous urban areas and can cause severe air pollution problems especially in wintertime. This study investigates wintertime winds in and around the Ulaanbaatar, the capital of Mongolia, metropolitan area in the presence of a temperature inversion using the Weather Research and Forecasting (WRF) model coupled with the Seoul National University Urban Canopy Model (SNUUCM). Ulaanbaatar is located in complex terrain and in a nearly east-west-oriented valley. A wintertime scenario with clear skies, weak synoptic winds, and a temperature inversion under the influence of a Siberian high-pressure system is selected. Local winds are weak in the presence of the temperature inversion. In the daytime, weak mountain upslope winds develop, up-valley winds appear to be stronger in the urban area than in the surrounding areas, and channeling winds are produced in the main valley. The bottom of the temperature inversion layer rises up in the urban area, and winds below the bottom of the temperature inversion layer strengthen. In the nighttime, mountain downslope winds and down-valley winds develop. Urban effects in the presence of the temperature inversion are examined by comparing the results of simulations with and without the city. It is shown that in the daytime the urban area acts to elevate the bottom of the temperature inversion layer and weaken the strength of the temperature inversion layer. Winds east of the city weaken in the afternoon and down-valley winds develop later in the simulation with the city.

**Key words:** Temperature inversion, wintertime winds, Ulaanbaatar, WRF model, urban canopy model

### 1. Introduction

Under clear skies and weak winds associated with high-pressure systems, the temperature inversion layer in which the temperature increases with height can form in complex terrain (Gerelchuluun and Ahn, 2014). Temperature inversions tend to persist longer in wintertime and in deep valleys (Whiteman, 1982; Kelly, 1988; Colette et al., 2003). Surface-based temperature inversions can be destroyed by surface heating, leading to elevated inversions. The strength of a temperature inversion layer is correlated with its thickness and decreases

with increasing surface temperature (Bradley et al., 1992) if the temperature at the inversion top changes little.

Topography in a mountainous city and its surrounding areas can act to reduce the exchange of the valley air with the surrounding and/or upper air. Whiteman et al. (1999) noted that the temperature inversion in wintertime, once formed in the basin, can persist for a multiday period and that the stable basin atmosphere tends to be isolated from the atmosphere aloft with relatively strong prevailing winds. The persistent temperature inversion often results in poor air quality in cities located in complex terrain (e.g., Malek et al., 2006; Olofson et al., 2009; Jung et al., 2010; Li et al., 2012).

Cities can induce and/or modify local circulations. Lee and Kim (2008) carried out numerical experiments of local circulations in the Daegu, South Korea, metropolitan area to examine the changes in local meteorology due to urbanization over 40 years. They showed that the daily mean temperature has increased and that mountain-valley winds have been modified. Using a numerical model, Ryu and Baik (2013) examined daytime local circulations (urban-breeze, sea-breeze, cross-valley, and river-breeze circulations) and their interactions in the Seoul, South Korea, metropolitan area. They showed that the urban breeze circulation effectively influences the cross-valley circulation. Generally, numerical studies of local circulations have thus far mainly considered favorable conditions for the development of local circulations. The presence of a temperature inversion is not favorable for the development of deep local circulations because the vertical extension of local circulations/winds is hindered by strong stratification. Temperature inversions especially in wintertime are frequent in mountainous cities. It is therefore interesting to investigate local circulations/winds in mountainous cities and the impacts of cities on local circulations/winds in the presence of a temperature inversion.

Ulaanbaatar, the capital of Mongolia, is located at an elevation of ~1350 m in a nearly east-west-oriented valley between the southern base of branches of the Khentiin Nuruu mountain range (with a maximum height of approximately 2800 m) and the northern base of Mt. Bogd Khan (with a maximum height of approximately 2200 m) (see Fig. 1b). In wintertime, the Siberian high-pressure system is dominant in Mongolia and this condition is favorable for the formation of a

Corresponding Author: Gantuya Ganbat, Information and Research Institute of Meteorology, Hydrology and Environment, Ulaanbaatar, Mongolia.  
E-mail: gantuya@snu.ac.kr

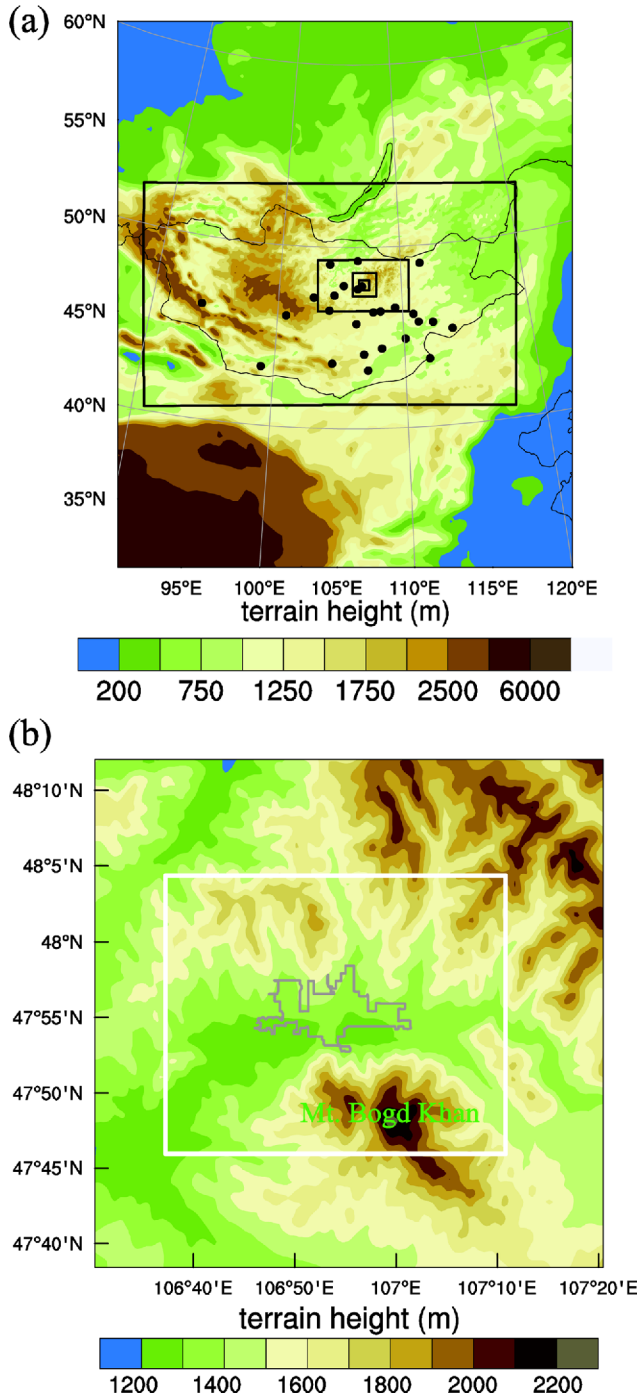


**Fig. 1.** Terrain height in the (a) five computational domains and (b) innermost domain. The white rectangle in (b) indicates the analysis area. 26 meteorological stations are indicated by the black dots in (a). The urban boundary is indicated by the gray line in (b).

temperature inversion in the complex terrain. Baasankhuu and Gomboluudev (1996) revealed from the observational data at Ulaanbaatar radiosonde station over the period of 1976-1985 that the monthly-averaged surface-based temperature inversion in Ulaanbaatar is strongest and deepest in December reaching  $6.9^{\circ}\text{C}$  strength and 809 m thickness. Gerelchuluun and Ahn

(2014) analyzed the strength and thickness of the temperature inversion layer in Mongolia using radiosonde data over the period of 1981-2010. Recently, Ganbat and Baik (2015) numerically investigated summertime local circulations in and around the Ulaanbaatar metropolitan area. They showed that local circulations in the daytime are characterized by mountain upslope winds, up-valley winds, and urban breezes, while local circulations in the nighttime are characterized by mountain downslope winds and channeling down-valley winds. Furthermore, they showed that the local circulations are sensitive to atmospheric stability and that the increase in atmospheric stability weakens daytime cross-valley winds and suppress the growth of the atmospheric boundary layer.

In this study, wintertime winds in and around the Ulaanbaatar metropolitan area in the presence of a temperature inversion are investigated using a mesoscale model coupled with an advanced urban canopy model. Section 2 presents a description of the model and experimental design. In section 3, the synoptic weather is described and the model is validated against observations. The results are presented and discussed in section 4. A summary and conclusions are given in section 5.

## 2. Model description and experimental design

The Weather Research and Forecasting (WRF) model version 3.2 (Skamarock et al., 2008) coupled with the Seoul National University Urban Canopy Model (SNUUCM) (Ryu et al., 2011) is employed for this study. The following physical parameterization schemes are used: the Dudhia shortwave radiation scheme (Dudhia, 1989), the Rapid Radiative Transfer Model (RRTM) longwave radiation scheme (Mlawer et al., 1997), the Yonsei University (YSU) planetary boundary layer scheme (Hong et al., 2006), the updated Kain-Fritsch cumulus parameterization scheme (Kain, 2004), and the Purdue Lin cloud microphysics scheme (Lin et al., 1983). The SNUUCM is coupled with the Noah land surface model (Chen and Dudhia, 2001), and it includes important physical processes that occur in urban canopies, such as absorption and reflection of shortwave and longwave radiation, turbulent energy and water exchanges between surfaces (roof, walls, and road), and heat conduction in the substrates. Following Ganbat and Baik (2015), some urban parameters in the SNUUCM for Ulaanbaatar are specified as follows. The built-up area fraction is 70%, and the natural area fraction is 30%. The building height is 10 m, and the canyon aspect ratio is 0.5. The albedos of roof, wall, and road are 0.12, 0.12, and 0.08, respectively. The diurnally varying anthropogenic heat is included. The maximum anthropogenic heat is  $20 \text{ W m}^{-2}$ , and its minimum is  $9 \text{ W m}^{-2}$ . The WRF model coupled with the SNUUCM has been successfully used to simulate local circulations in metropolitan areas (Ryu and Baik, 2013; Ganbat and Baik, 2015).

Five computational domains with two-way nesting are considered (Fig. 1a). The numbers of horizontal grid points for the five computational domains are  $110 \times 125$ ,  $247 \times 148$ ,  $181 \times$

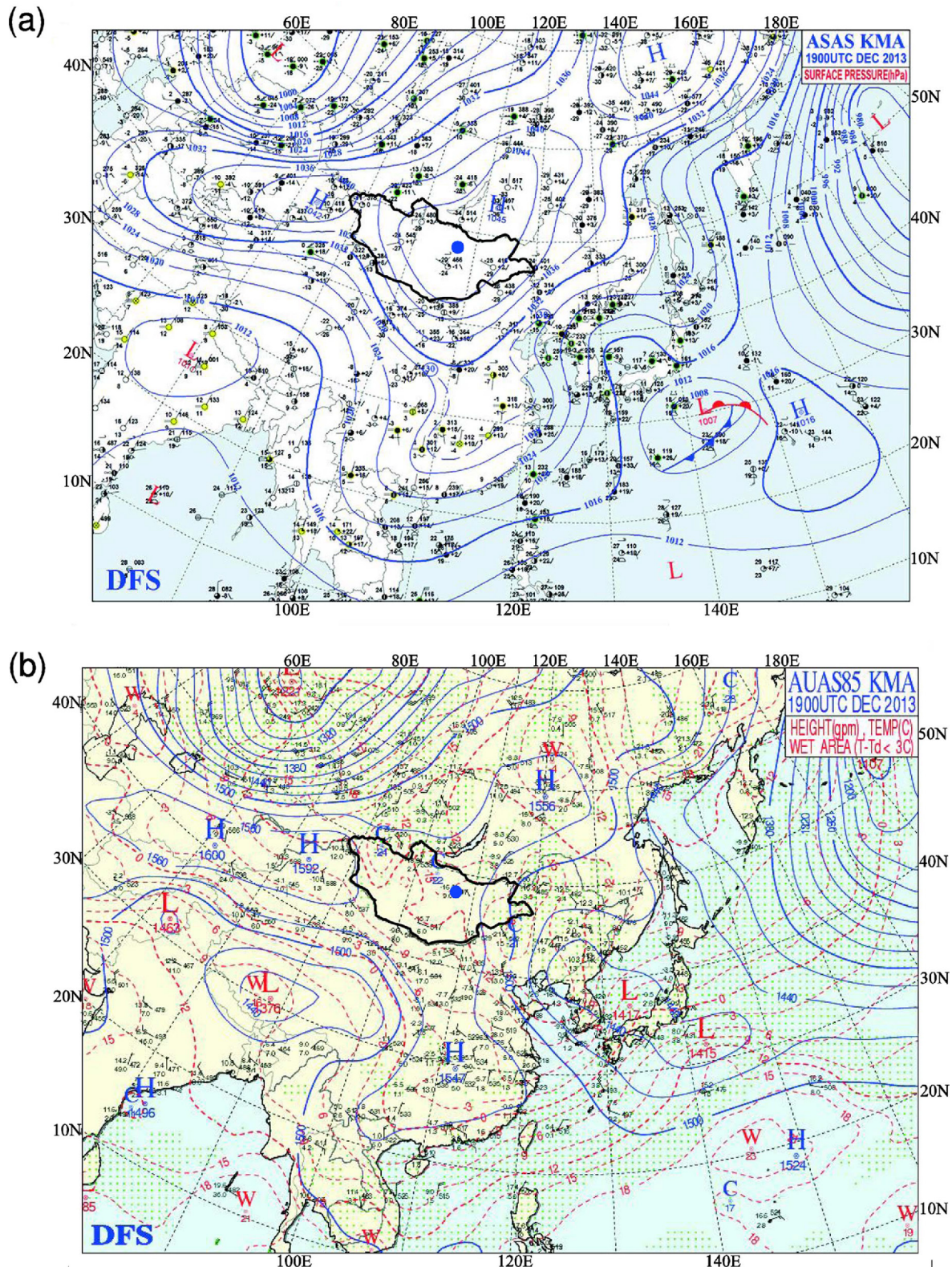


**Fig. 2.** (a) Surface and (b) 850 hPa weather maps at 0000 UTC (0800 LST) 19 December 2013 (courtesy of the Korea Meteorological Administration). The boundary of Mongolia is indicated by the black solid line, and Ulaanbaatar is indicated by the blue circle. In (a), the blue lines are isobars with contour intervals of 4 hPa. In (b), the blue lines are constant geopotential height lines with contour intervals of 30 m, the red dashed lines are isotherms with contour intervals of 3°C, and the green dotted areas represent wet areas in which the temperature minus the dew point temperature is less than 3°C.

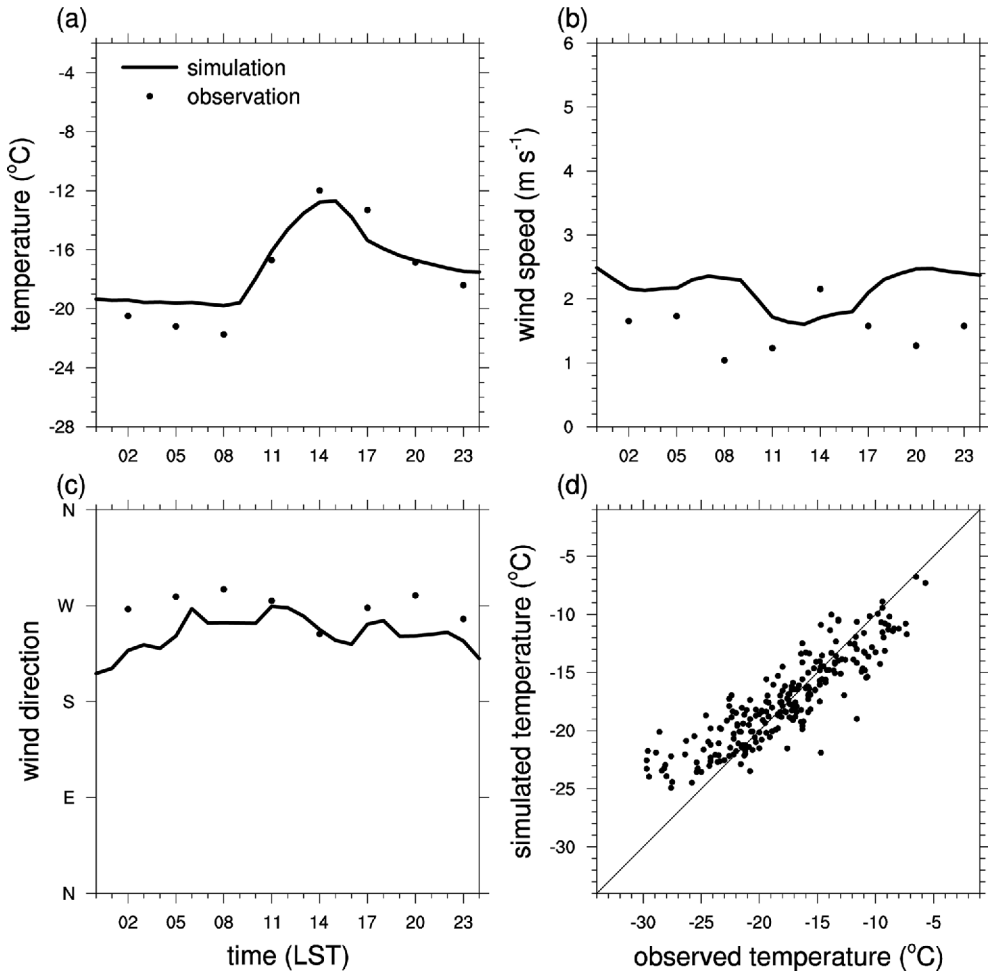


**Fig. 3.** Diurnal variations of observed and simulated (a) 2-m temperature, (b) 10-m wind speed, (c) 10-m wind direction, and (d) scatterplot of 2-m temperatures observed at 26 meteorological stations and simulated. Observations are made at 3-h intervals. The time series are averages over 26 stations/grid points.

103, 142 × 142, and 181 × 181 with horizontal grid intervals of 27, 9, 3, 1, and 1/3 km, respectively. The vertical grid spacing is stretched with height, and the number of vertical layers is 50 with a lowest model level of ~12 m. The cumulus parameterization scheme is applied to the outer two computational domains with horizontal grid intervals of 27 and 9 km. The National Centers for Environmental Prediction (NCEP) final analysis data with a horizontal resolution of  $1^\circ \times 1^\circ$  in 6-h intervals are used for initial and boundary conditions. The model is integrated for 28 h starting from 1200 UTC (2000 LST) 18 December 2013, and data from the last 24 h are used for the analysis. Note that the temperature inversion layer is already present at the time of initialization. Terrain data from the Shuttle Radar Topography Mission (SRTM) data with a resolution of ~90 m (Jarvis et al., 2008) provide a good representation of topography for the study area (Fig. 1b). The land-use/land-cover data consist of the United States Geological Survey (USGS) data (30" resolution). For Ulaanbaatar, in addition to the USGS data, the Moderate Resolution Imaging

Spectroradiometer (MODIS) data (~1 km resolution) (Friedl et al., 2002), the GlobCover land cover classifications map (~300 m resolution) (Arino et al., 2010), and the Google Earth imagery (Google Inc., 2013) are utilized.

To clearly examine urban effects on wintertime winds in and around the Ulaanbaatar area in the presence of the temperature inversion layer, an additional experiment (called the no-urban simulation) in which the urban area is replaced with a grassland land-cover type is performed and the results of the simulation without the city are compared with those of the simulation with the city. The grassland land-cover type is a typical land-cover category in surroundings of Ulaanbaatar.

### 3. Synoptic weather and model validation

Palfy (1995) and Whiteman et al. (1999) stated that the high-pressure system in wintertime is a favorable condition for the development of a temperature inversion. A Siberian high-pressure system dominated in the study area on 18–20

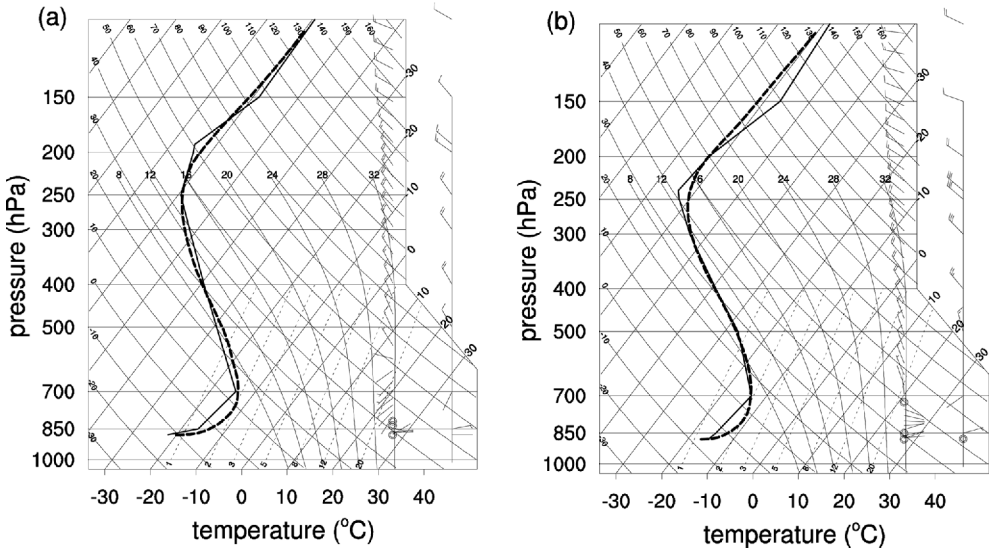


**Fig. 4.** Vertical profiles of observed and simulated temperatures and winds at Ulaanbaatar radiosonde station at (a) 0800 and (b) 2000 LST 19 December 2013. The solid thin lines indicate the observed temperatures, and the dashed thick lines indicate the simulated temperatures.

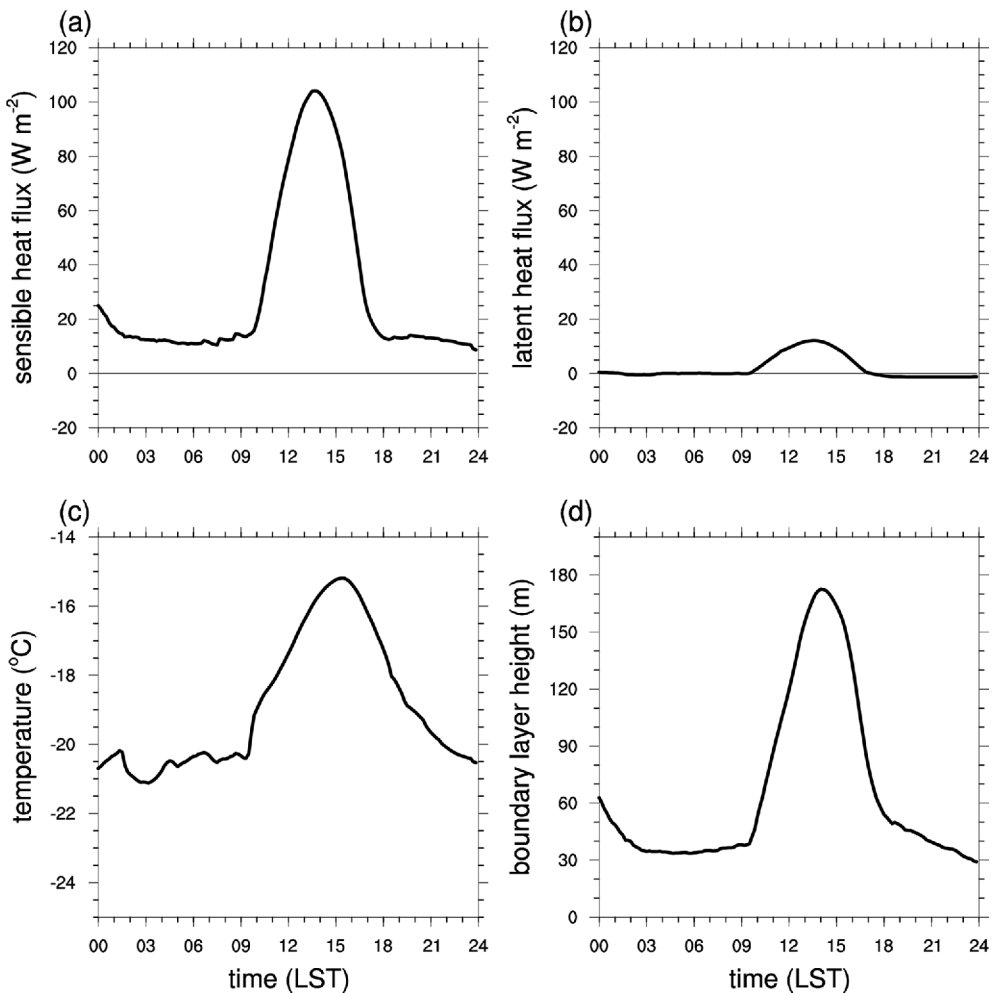


**Fig. 5.** Diurnal variations of (a) surface sensible heat flux, (b) surface latent heat flux, (c) 2-m temperature, and (d) boundary layer height averaged over the urban area.

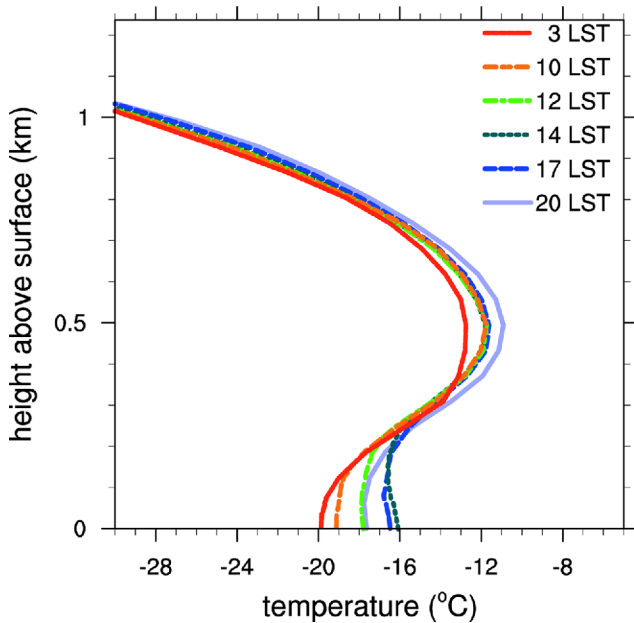


**Fig. 6.** Vertical profiles of temperature at 0300, 1000, 1200, 1400, 1700, and 2000 LST averaged over the urban area.

December 2013 (see the surface weather map in Fig. 2a). The upper level was under the influence of the large-scale ridge system (see the 850-hPa weather map in Fig. 2b). Wind speeds at 10 m observed at meteorological stations in and around Ulaanbaatar were  $0\text{--}3 \text{ m s}^{-1}$  on 19 December 2013. Wind speeds at 700 and 850 hPa were  $1\text{--}4 \text{ m s}^{-1}$  and skies were clear, thus the synoptic conditions were favorable for the formation of a temperature inversion in the complex terrain.

The simulated 2-m temperature and 10-m wind speed and direction in the computational domain with a 9-km horizontal grid interval are validated against observations at 26 meteorological stations (Figs. 3a-c). The observations in Figs. 3a-c are averaged over the 26 meteorological stations (Fig. 1a), and the simulation data in Figs. 3a-c are averaged over 26 corresponding grid points (nearest to the meteorological stations). The meteorological stations are indicated by black dots in Fig. 1a. In the simulation, the minimum temperature is overestimated and the maximum temperature is slightly underestimated, but the diurnal variation of temperature is well reproduced. The wind speed is slightly overestimated. To quantify the performance of the model, the hit rate is calculated. The accuracy ranges of hit rates for temperature, wind speed, and wind direction are set as  $\pm 2^\circ\text{C}$ ,  $1 \text{ m s}^{-1}$ , and  $30^\circ$ , respectively. The calculated hit rates for temperature, wind speed, and wind direction are 94.9%, 96.1%, and 83.1%, respectively, demonstrating a good performance. The mean bias errors of temperature, wind speed, and wind direction are  $-0.4^\circ\text{C}$ ,  $-0.6 \text{ m s}^{-1}$ , and  $30^\circ$ , respectively. The root-mean-square errors (RMSE) of temperature, wind speed, and wind direction are  $1.2^\circ\text{C}$ ,  $0.8 \text{ m s}^{-1}$ , and  $40^\circ$ , respectively. The scatterplot of observed and simulated 2-m temperatures shows a good agreement between the observations and simulation

(Fig. 3d). The diurnal variation of 2-m temperatures simulated in the computational domain with a 1/3-km horizontal grid interval is compared with that of observed 2-m temperatures at Ikh Surguuli station ( $47^\circ 55' 21.8''\text{N}$ ,  $106^\circ 55' 12.9''\text{E}$ ) which is located in Ulaanbaatar, showing a reasonable agreement.

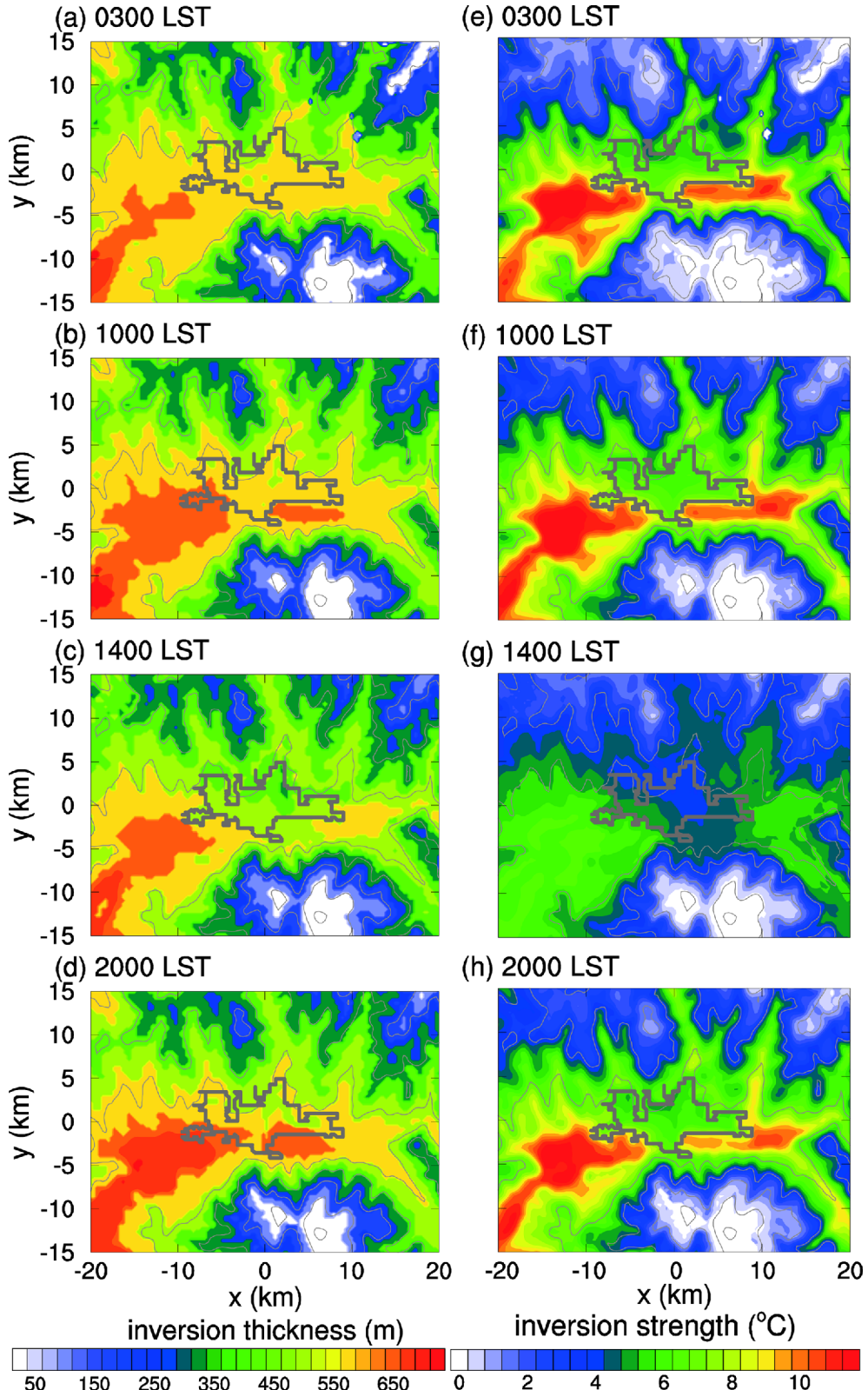
The vertical profiles of simulated temperatures and winds in the innermost domain are compared with those of observed temperatures at Ulaanbaatar radiosonde station ( $47^\circ 55' 4.4''\text{N}$ ,  $106^\circ 50' 52.3''\text{E}$ ) at 0800 and 2000 LST 19 December 2013 (Fig. 4). The radiosonde data are available only at standard levels, so a rigorous validation is limited. In spite of this, the simulated temperature and wind profiles are similar to the observed ones at both times.

#### 4. Results and discussion

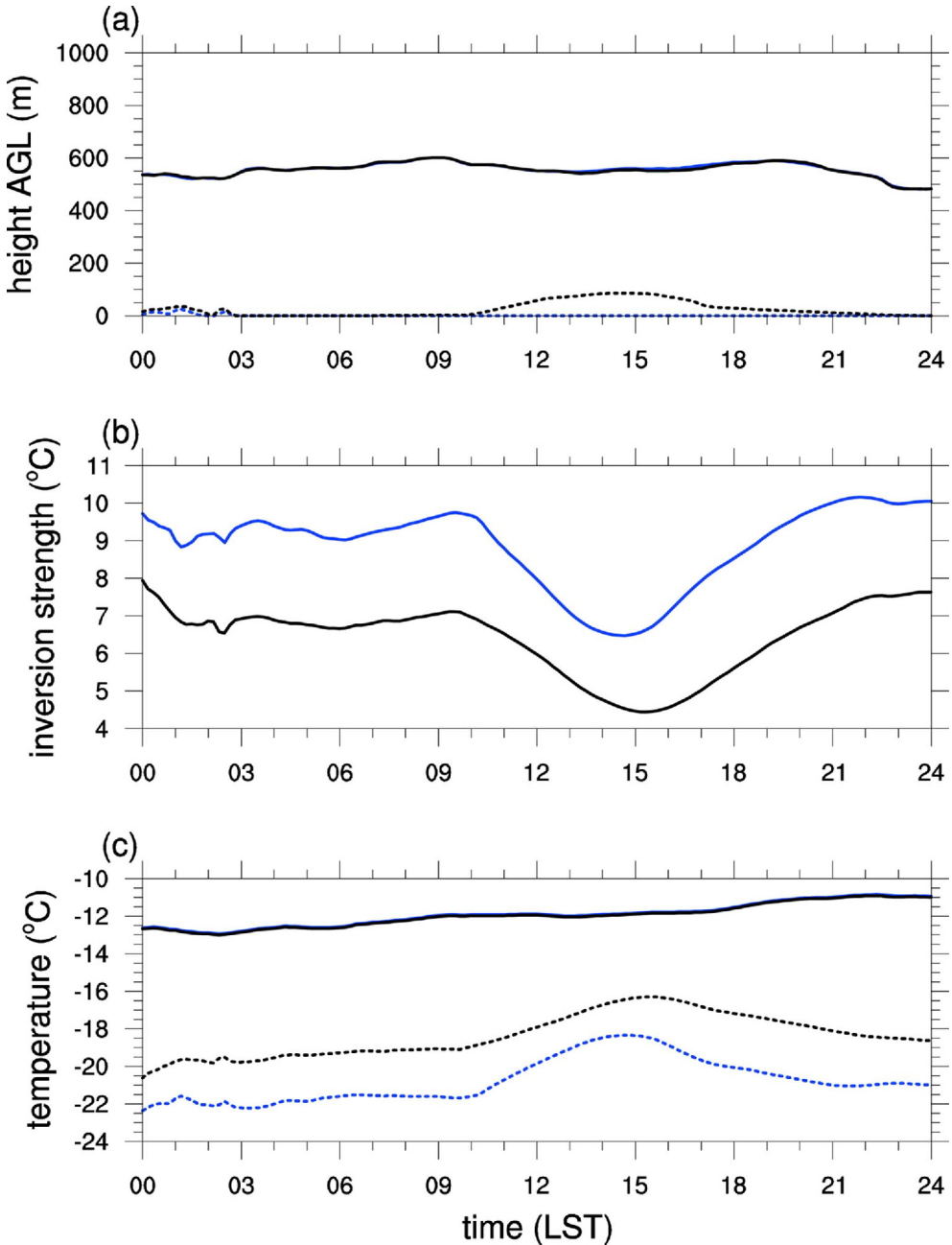
Figure 5 shows the diurnal variations of surface sensible heat flux, surface latent heat flux, 2-m temperature, and boundary layer height averaged over the urban area (see the area bounded by the gray line in Fig. 1b). In the YSU planetary boundary layer scheme, the boundary layer height is defined as the height at which minimum flux exists at the inversion level (Hong et al., 2006). Note that the simulated 2-m temperature averaged over the urban area is very low, ranging from  $-21^\circ\text{C}$  to  $-15^\circ\text{C}$ , and that local winds in a very cold environment are investigated in this study. The simulated wintertime surface sensible heat flux is smaller than the summertime one (Ganbat and Baik, 2015) and is always positive. The maximum surface sensible heat flux is  $104 \text{ W m}^{-2}$  at 1330 LST. The surface latent heat flux is much smaller than the surface sensible heat flux, which is a typical feature of urban areas (Grimmond et al., 2010). The maximum surface latent heat flux is  $12 \text{ W m}^{-2}$  at 1320 LST. In contrast with the summertime deep convective boundary layer (Ganbat and Baik, 2015), the growth of the boundary layer in wintertime is suppressed. The boundary layer grows only up to a maximum of 172 m in the daytime. The nighttime boundary layer is very shallow in the very stable atmosphere, consistent with previous studies (e.g., Mahrt and Vickers, 2006; Banta et al., 2007). In the very stable atmosphere, most of the surface sensible heat flux acts to reduce the large temperature lapse rate rather than acts to grow the boundary layer (Bader and McKee, 1985).

Figure 6 shows the vertical profiles of temperature at six different times averaged over the urban area. At 0300 and 1000 LST, the temperature increases from the surface up to  $\sim 500$  m and then decreases with height. At 1400 and 1700 LST, the layer in which the temperature increases with height is clearly elevated.

Figure 7 shows the fields of the thickness and strength of the temperature inversion layer in the analysis area (Fig. 1b). The selected times are 0300, 1000, 1400, and 2000 LST. In this study, the thickness of the temperature inversion layer is defined as its (the temperature inversion layer's) top height minus its bottom height, and the strength of the temperature inversion layer is defined as the temperature at its top minus



**Fig. 7.** Fields of the thickness (left) and strength (right) of the temperature inversion layer at (a), (e) 0300, (b), (f) 1000, (c), (g) 1400, and (d), (h) 2000 LST. The light gray lines (also in Figs. 9, 12, and 13) indicate terrain height contours (from 1400 to 2200 m with intervals of 200 m). The urban boundary is indicated by the dark gray line (also in Figs. 9, 12, 13, and 14). Note that Fig. 7 (also Figs. 9, 12, 13, and 14) is for the analysis area.



**Fig. 8.** Diurnal variations of (a) top and bottom heights of the temperature inversion layer, (b) its strength, and (c) temperatures at the inversion top and bottom averaged over the urban area (black solid and short-dashed lines). The blue solid and short-dashed lines are for the no-urban simulation, and the heights, the strength, and the temperatures are averaged over the same area.

the temperature at its bottom. Figure 7 indicates that the temperature inversion is persistent over time and that the thickness and strength of the temperature inversion layer generally follow the terrain. The temperature inversion layer is deep and strong in the valleys, particularly in the wide valley located southwest of the domain. On the other hand, the temperature inversion layer is relatively shallow and weak over the mountain slopes and does not exist over and around the high mountain peaks. The areas with the deep temperature

inversion seem to be matched with low terrain features. The height of the valley floor affects the thickness of the temperature inversion layer. An in-depth investigation is needed to quantify the effect of the valley floor height on the temperature inversion. The temperature inversion layer is shallower and its strength is weaker in the urban area than in its nearby valley area. This is due to urban effects. It is observed that the temperature inversion in the valleys except for the urban area and over the mountain slopes is mostly surface-based and its

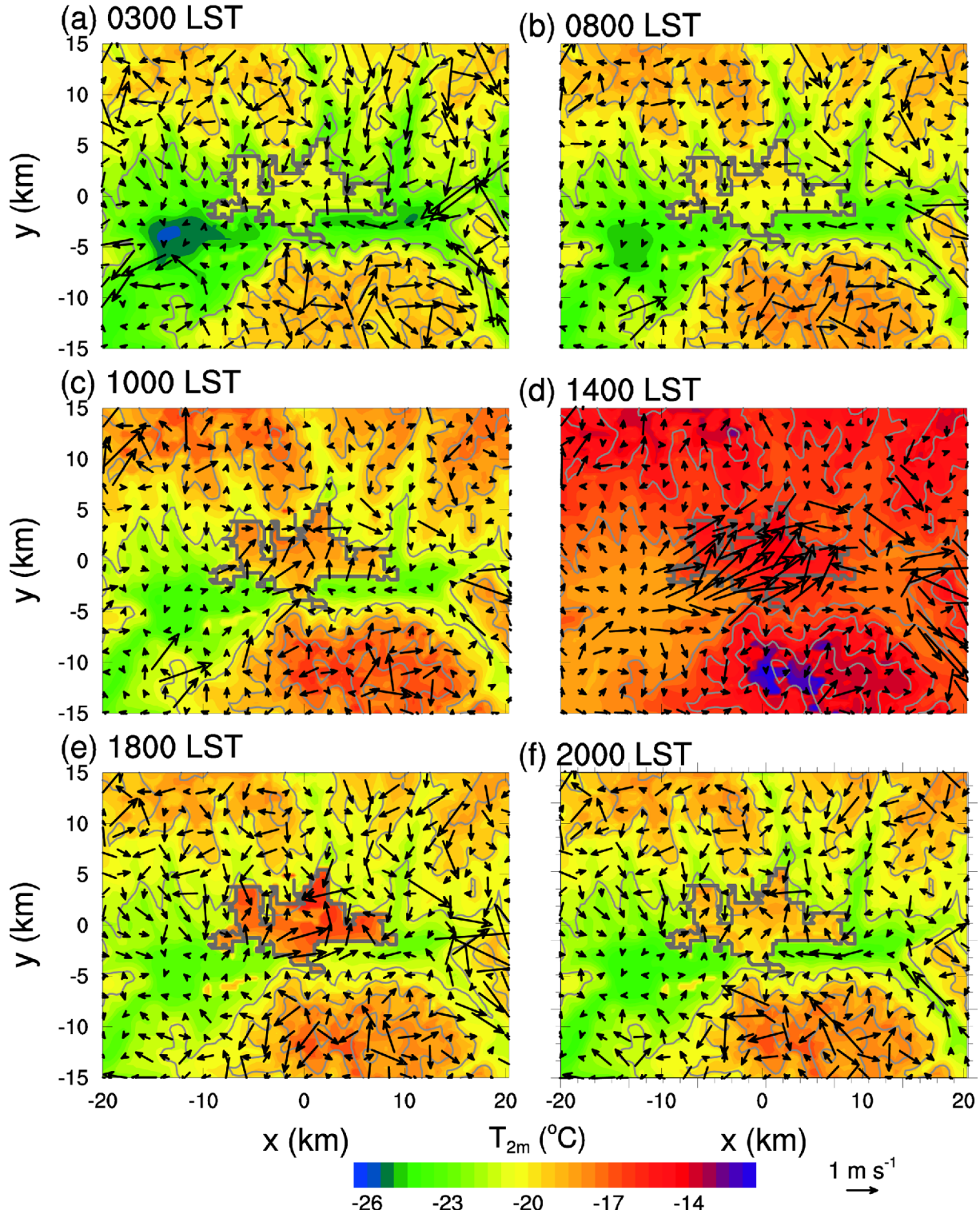


**Fig. 9.** Fields of 2-m temperature and 10-m wind vector at (a) 0300, (b) 0800, (c) 1000, (d) 1400, (e) 1800, and (f) 2000 LST.

thickness and strength vary diurnally (figure not shown). It is also observed that the bottom of the temperature inversion layer lies below the top of the boundary layer and that the top of the temperature inversion layer is lower than the maximum ridge top of the surrounding mountains.

Figure 8 shows the diurnal variations of top and bottom heights of the temperature inversion layer, its strength, and temperatures at the inversion top and bottom averaged over the urban area. The temperature inversion is not surface-based in the daytime, and the top of the temperature inversion layer

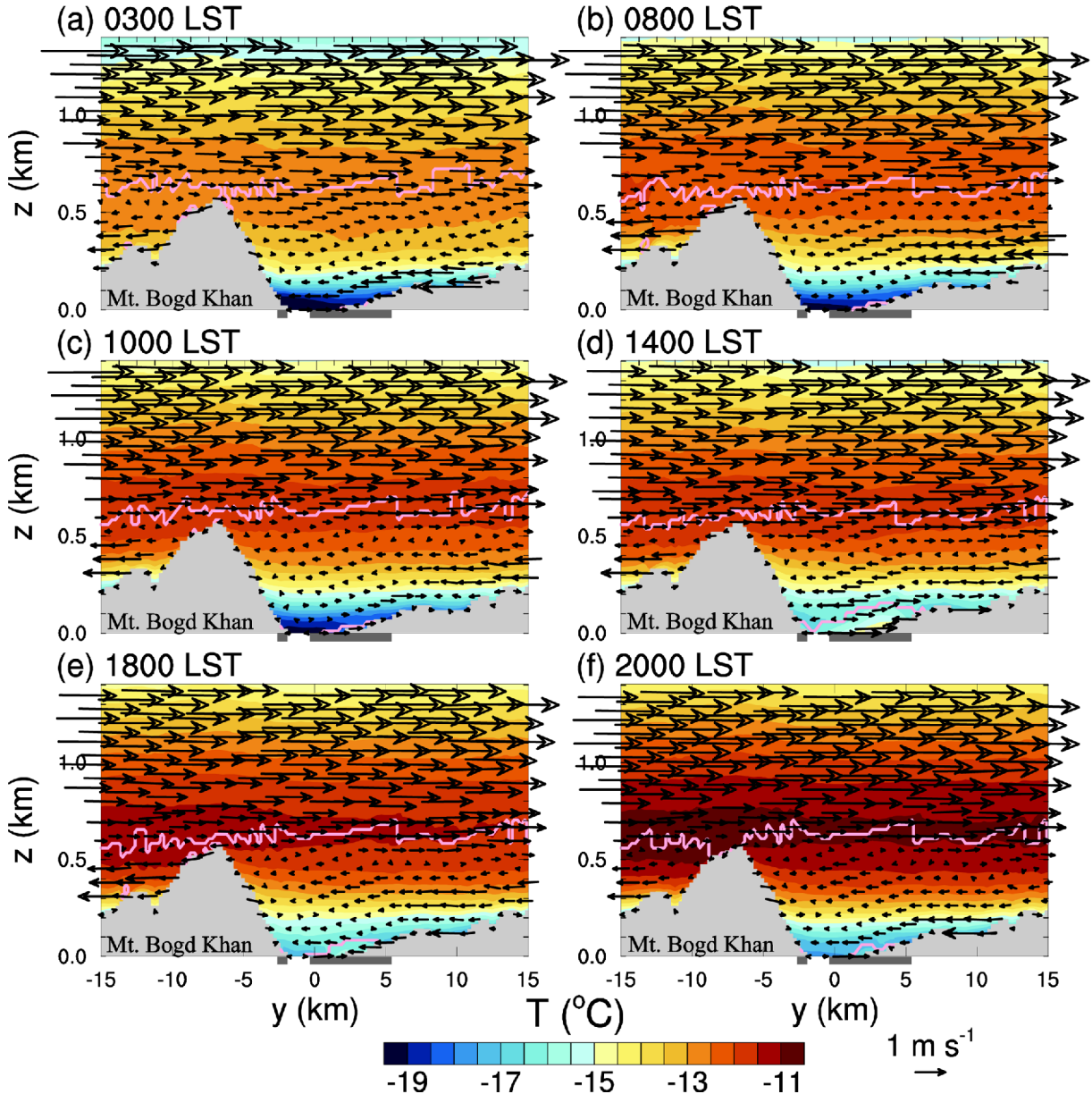


**Fig. 10.** Vertical cross-sections of temperature and wind vector along the north-south direction at  $x = 0$  km at (a) 0300, (b) 0800, (c) 1000, (d) 1400, (e) 1800, and (f) 2000 LST. The gray boxes on the horizontal axis indicate the urban area, and pink lines indicate the boundary where the vertical temperature gradient changes its sign (also in Fig. 11).

averaged over the urban area varies little over time. The bottom of the temperature inversion layer averaged over the urban area varies between 0 and 86 m, and its top height varies between 481 and 601 m. The thickness of the temperature inversion layer averaged over the urban area ranges 462–599 m. The simulated thickness of the temperature inversion layer is comparable to the December average ( $\sim 650$  m) over the period of 1981–2010 at Ulaanbaatar radiosonde station (Gerelchuluun and Ahn, 2014). The temperature inversion strength averaged over the urban area decreases from 0930 LST ( $7.1^{\circ}\text{C}$ ) to 1520 LST ( $4.4^{\circ}\text{C}$ ) (Fig. 8b) and then increases. As the urban surface heats, the bottom of the temperature inversion layer heats and

rises up, while its top changes little. This causes the strength of the temperature inversion layer to weaken (Figs. 8b, c). The destruction of the temperature inversion layer, which is associated with the growth of the convective boundary layer with time while the inversion top remains almost fixed in time, is identified as Pattern 1 by Whiteman (1982).

Next, local winds in the presence of the temperature inversion are examined by analyzing simulated temperature and wind fields. Figure 9 shows 2-m temperature and 10-m wind vector fields. The selected times are 0300, 0800, 1000, 1400, 1800, and 2000 LST. Figure 10 (Figure 11) shows the vertical cross-sections of temperature and wind vector along

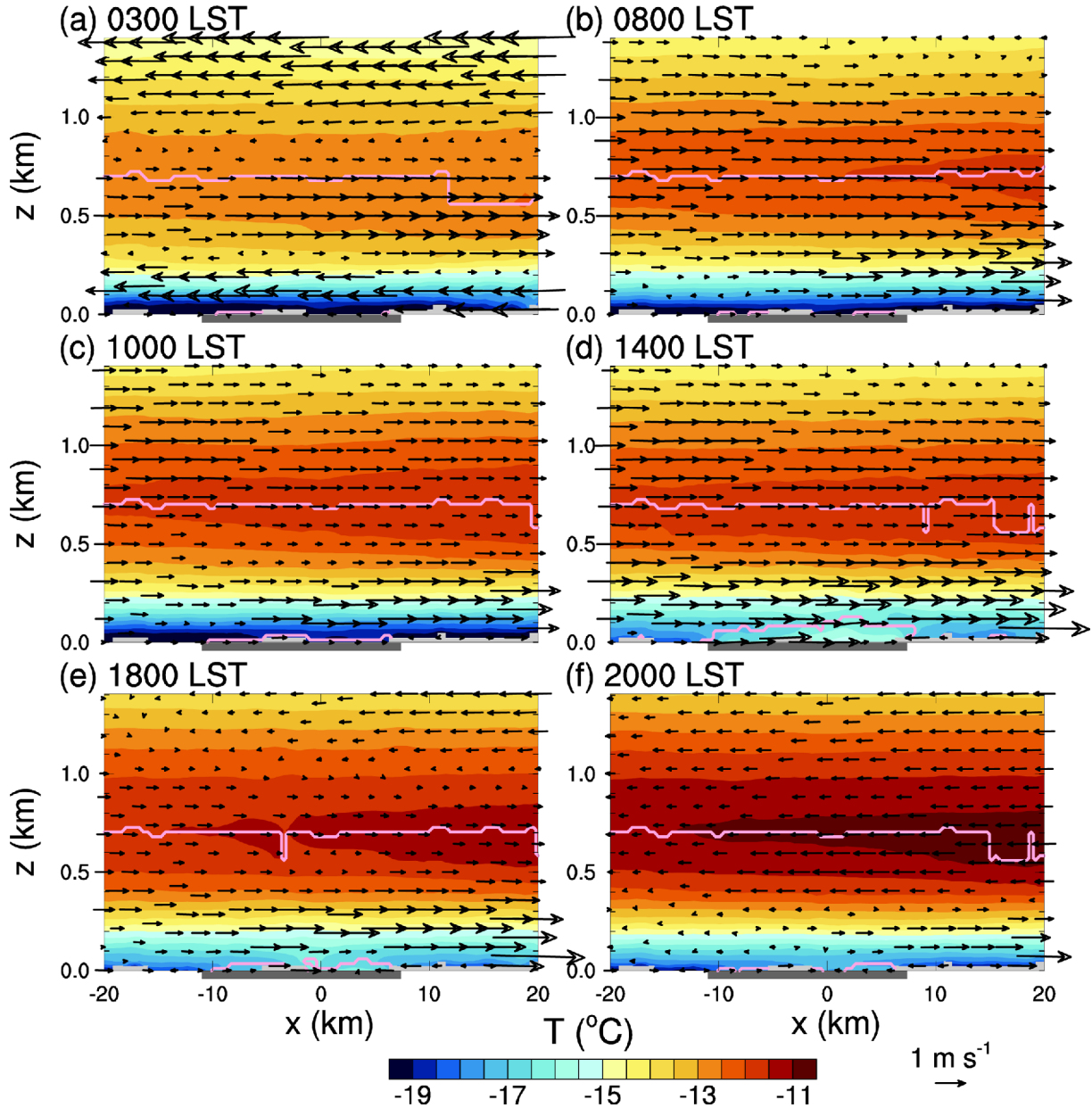


**Fig. 11.** Vertical cross-sections of temperature and wind vector along the east-west direction at  $y = 0$  km at (a) 0300, (b) 0800, (c) 1000, (d) 1400, (e) 1800, and (f) 2000 LST.

the north-south direction (along the east-west direction) at  $x = 0$  km (at  $y = 0$  km) at same times as in Fig. 9.

At 0300 LST, the temperature in the urban area is higher than that in its surrounding valley areas, exhibiting an urban heat island phenomenon (Fig. 9a). Weak mountain downslope winds and weak down-valley winds are seen. Weak converging winds are present in the urban area, which are largely due to the urban heat island-induced flow, that is, the urban breeze (Fig. 9a). In addition to the urban breeze, it is observed that down-valley winds from the tributary valleys to the north are partly responsible for the weak converging winds in the urban area. Down-valley winds up to  $z \sim 250$  m above the surface

blow down the valley (easterly), featuring channeling winds (Fig. 11a). Channeling winds are characterized by winds in a valley predominantly parallel to the valley axis (e.g., Whiteman and Doran, 1993; Eckman, 1998). Winds in the temperature inversion layer seem to be to some extent decoupled from stronger upper-level southerly-component winds (Fig. 10a). This is consistent with the results of Whiteman and McKee (1977). At 0800 LST, the temperature inversion layer is still deep in the urban area (Figs. 10b and 11b) and near-surface down-valley winds weaken or disappear (Fig. 9b). Note that on this particular day, in Ulaanbaatar, civil twilight began at 0801 LST and the sunrise time was at 0838 LST. At 1000 LST, up-

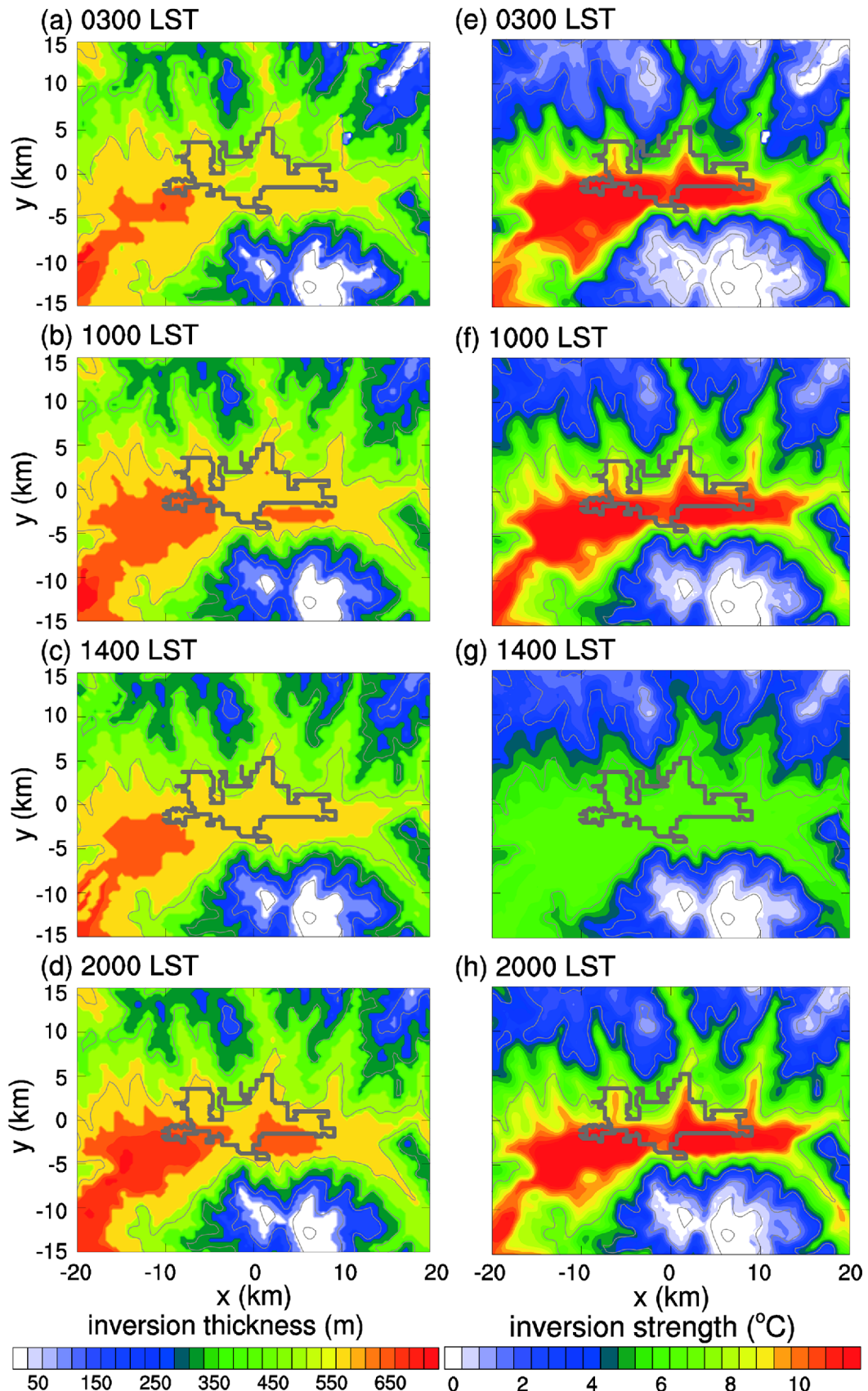


**Fig. 12.** Same as in Fig. 7 but for the no-urban simulation.

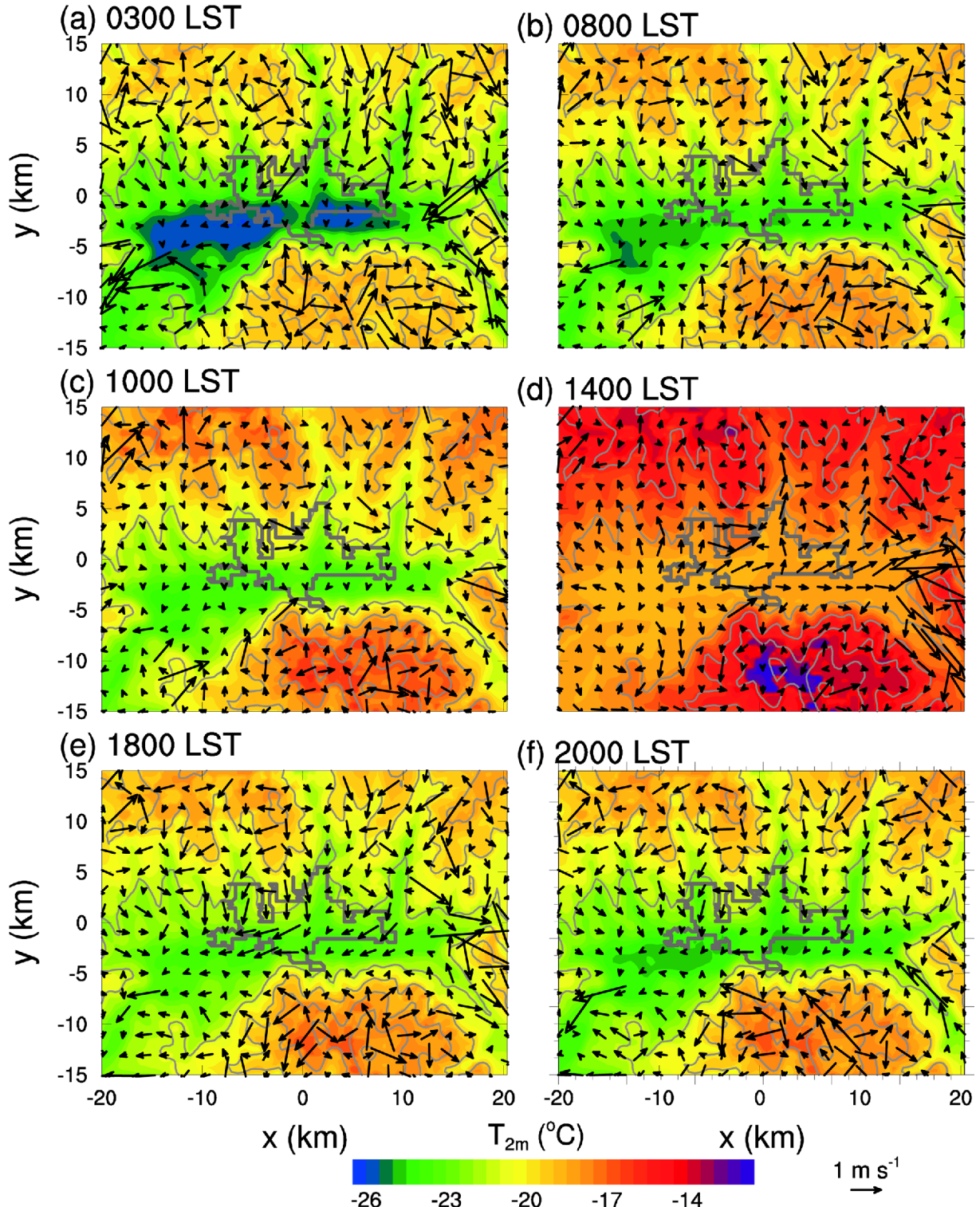


**Fig. 13.** Same as in Fig. 9 but for the no-urban simulation.

valley winds form (Figs. 9c and 11c). The temperature inversion bottom in the urban area slightly rises up, and winds are stronger in the urban area than in the surrounding valley floor (Figs. 9c, 10c, and 11c). At 1400 LST, in the urban area the temperature inversion bottom further rises up, exhibiting an

elevated temperature inversion layer, and up-valley winds strengthen (Figs. 9d, 10d, and 11d). East of the city, the urban breeze blows toward the city (easterly winds), while valley winds blow in the up-valley direction (westerly winds), resulting in weakened near-surface winds. At 1800 LST,

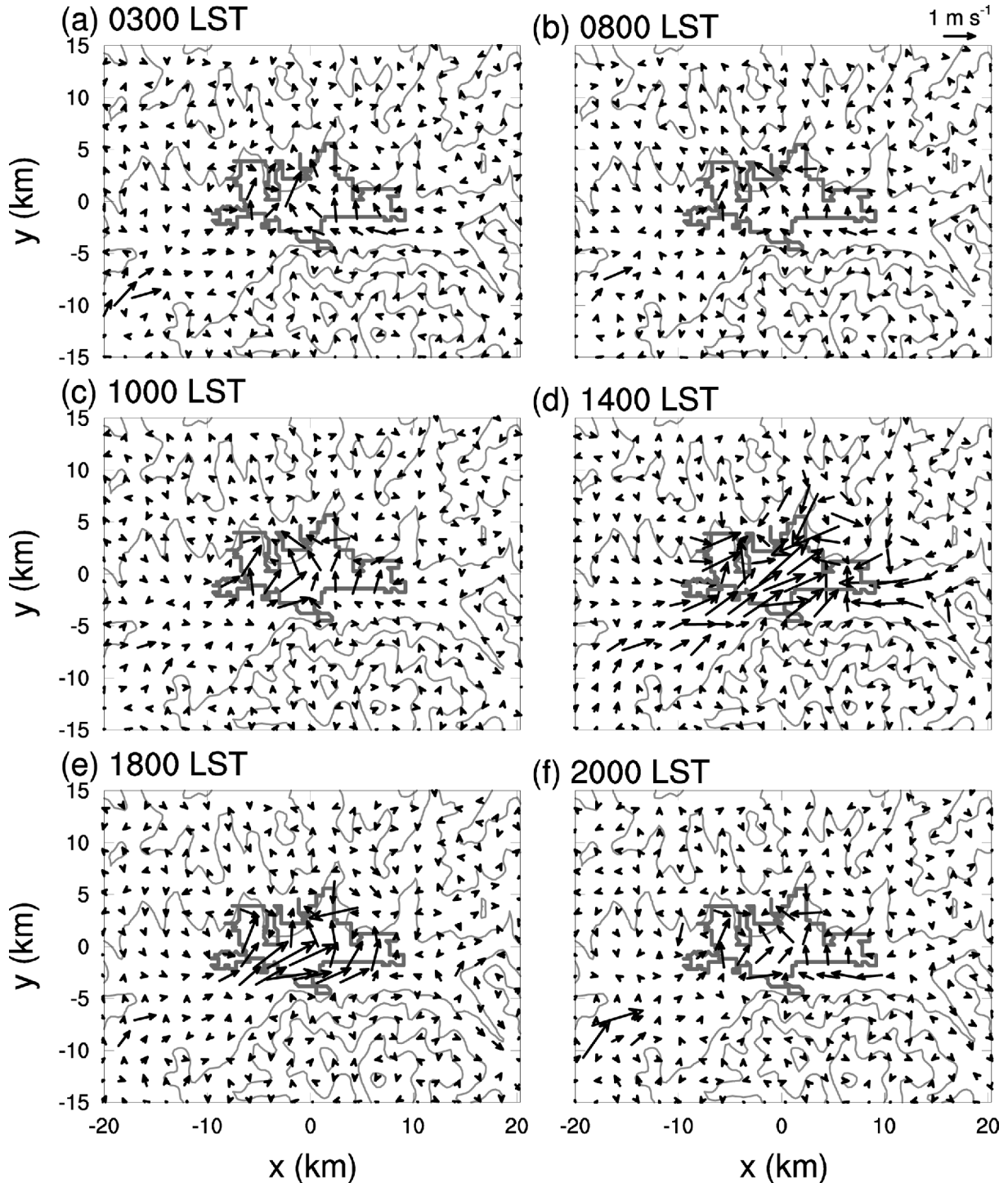


**Fig. 14.** Fields of difference in 10-m wind vector between the control and no-urban simulations at (a) 0300, (b) 0800, (c) 1000, (d) 1400, (e) 1800, and (f) 2000 LST.

mountain downslope winds develop, the temperature inversion bottom in the urban area descends, and winds below the temperature inversion bottom weaken (Figs. 9e, 10e, and 11e). At 2000 LST, mountain downslope winds and down-valley winds become stronger (Fig. 9f).

To examine urban effects on local winds in the presence of

the temperature inversion, an experiment is conducted in which the urban area is replaced by the grassland land-cover type (no-urban simulation) and the results are compared to those of the simulation with the urban area (called the control simulation). Figure 12 shows the fields of the thickness and strength of the temperature inversion layer at 0300, 1000,

1400, and 2000 LST in the no-urban simulation. In Ulaanbaatar, the thickness of the temperature inversion layer is smaller and its intensity is weaker in the control simulation than in the no-urban simulation (Figs. 7 and 12), showing urban effects on the temperature inversion layer as seen more clearly in Fig. 8. In Ulaanbaatar, the height of the temperature inversion layer top and its temperature are almost the same in both the simulations, and the temperature at the bottom of the temperature inversion layer is higher in the control simulation than in the no-urban simulation because of the urban surface forcing (Fig. 8). This leads to weaker temperature inversion layer in the control simulation than in the no-urban simulation.

Figure 13 shows the fields of 2-m temperature and 10-m wind vector at 0300, 0800, 1000, 1400, 1800, and 2000 LST in the no-urban simulation. Figure 14 shows the fields of difference in 10-m wind vector between the control and no-urban simulations at 0300, 0800, 1000, 1400, 1800, and 2000 LST. At 0300 and 0800 LST, the temperature difference between the control and no-urban simulations in the urban area is large (up to 5.0°C and 4.4°C at 0300 and 0800 LST, respectively) and down-valley winds in the main valley region are slightly stronger in the control simulation than in the no-urban simulation (Figs. 9a, b and 13a, b). At 1000 LST, weak converging winds are present in and east of Ulaanbaatar in the control simulation (Fig. 9c), but these are almost absent in the no-urban simulation (Fig. 13c). The difference in wind field in Ulaanbaatar becomes clear at 1000 LST (Fig. 14c). At 1400 LST, up-valley winds in Ulaanbaatar are stronger in the control simulation than in the no-urban simulation (Figs. 9d and 13d). The interactions of up-valley winds with urban breezes lead to stronger up-valley winds in Ulaanbaatar. It is also seen that winds east of the city weaken in the control simulation due to counteracting urban breezes (Figs. 9d and 13d). The difference in wind field in Ulaanbaatar is larger at 1400 LST than at 1000 LST (Figs. 14c, d), meaning stronger urban breezes at 1400 LST. Note that while the urban forcing increases in the daytime, the bottom of the temperature inversion rises up and the layer below it becomes less stable leading to an increase in wind speed over the urban area in the control simulation. At 1800 LST, in Ulaanbaatar, up-valley winds are still present in the control simulation, while down-valley winds already develop in the no-urban simulation (Figs. 9e and 13e). The delay of the development of down-valley winds in the control simulation is associated with urban breezes. Urban breezes in the control simulation are weaker at 1800 LST than at 1400 LST (Figs. 14d, e). At 2000 LST, winds in Ulaanbaatar are slightly stronger in the control simulation than in the no-urban simulation (Figs. 9f and 13f).

The simulated wintertime winds in and around the Ulaanbaatar metropolitan area are weaker than the summertime local circulations/winds examined by Ganbat and Baik (2015). This is attributed to the presence of the temperature inversion and smaller surface sensible heat flux. Although the simulated wintertime local winds are weaker, urban breezes, mountain slope winds, and valley winds develop and the

interactions of urban breezes with up-/down-valley winds occur clearly.

In this study, the 28-h integration is performed starting from 2000 LST 18 December and the last 24-h data are used for the analysis. Note that the experiment with a longer spin-up time showed a slightly lower performance than the current experiment in the present case study. Due to the absence of daytime spin-up, the nighttime urban heat island intensity (e.g., 0300 LST, Fig. 9a) is likely underestimated in this study. Longer spin-up time that includes daytime spin-up is needed to better simulate nighttime urban heat islands (Hu et al., 2013b). The issue of spin-up time in high-resolution, wintertime simulations in complex terrain deserves an investigation.

Many previous studies have indicated that simulated boundary layer structure and near-surface temperatures/winds are sensitive to planetary boundary layer schemes (e.g., Hu et al., 2010; LeMone et al., 2014). Nonlocal planetary boundary layer schemes tend to produce some biased nocturnal winds due to unrealistic, strong momentum mixing in the nighttime (Hu et al., 2010, 2013b). It would be interesting to examine the sensitivity of thermal and wind environment to planetary boundary layer schemes in and around the Ulaanbaatar metropolitan area, particularly focusing on the performances of local and nonlocal mixing schemes in the stable boundary layer. It is noted that the YSU planetary boundary layer scheme in the WRF model version 3.2 used in this study has been updated. An update for the stable boundary layer shows positive impacts on simulated near-surface temperatures/winds (Hu et al., 2013a). Thus, using the recent WRF model version with the updated YSU planetary boundary layer scheme could lead to more realistic simulation of thermal and wind environment in and around the Ulaanbaatar metropolitan area, deserving an investigation.

## 5. Summary and conclusions

Wintertime winds in the presence of a temperature inversion in and around the Ulaanbaatar metropolitan area were studied using the mesoscale model coupled with the advanced urban canopy model. The thickness and strength of the temperature inversion layer were found to be associated with the terrain. The persistent temperature inversion layer is deep in the valleys and shallow over the mountain slopes. Local winds, which include urban breezes, mountain slope winds, and up-and down-valley winds, were found to be weak in the presence of the temperature inversion. In the daytime, mountain upslope winds are weak, up-valley winds strengthen in the urban area, and near-surface winds east of the city are weak. As the temperature inversion bottom rises up in the urban area, winds below the temperature inversion bottom strengthen. In the nighttime, downslope winds and down-valley winds develop.

Urban effects on local winds in the presence of the temperature inversion were examined. In the daytime, the temperature inversion layer becomes shallower and weaker in Ulaanbaatar in the control simulation than in the no-urban simulation. The

absence of urban breezes in the no-urban simulation results in weaker up-valley winds in the main valley and stronger up-valley winds east of the city than in the control simulation. Down-valley winds in the main valley starts earlier in the no-urban simulation because of the absence of urban breezes.

Temperature inversion layers have important implications to air pollution in wintertime. Under clear skies and weak synoptic winds associated with Siberian high-pressure systems, emitted pollutants are trapped in the boundary layer, causing severe air pollution problems in Ulaanbaatar. Field studies as well as further numerical modeling studies for the Ulaanbaatar metropolitan area are needed to enhance our understanding of local circulations and air pollution in the presence of a temperature inversion. Furthermore, it would be worthwhile to investigate the formation and breakup of a temperature inversion layer in the valley city.

**Acknowledgments.** The authors are grateful to two anonymous reviewers for providing valuable comments on this work. This study was supported by the Korea Meteorological Administration Research and Development Program under Grant KMIPA 2015-5100 and also by the National Research Foundation of Korea (NRF) grant funded by the Korea Ministry of Science, ICT and Future Planning (MSIP) (2011-0017041). The first author is partly supported by the Asia Research Center, Mongolia and Korea Foundation for Advanced Studies, Korea within the framework of the project “Numerical simulations of the relationship between atmosphere, dust storms, and land surface characteristics in Gobi area, Mongolia”.

**Edited by:** Jimy Dudhia

## REFERENCES

- Arino, O., J. Ramos, V. Kalogirou, P. Defourny, and F. Achard, 2010: GlobCover 2009. ESA Living Planet Symposium, Bergen, Norway, ESA, SP-686.
- Baasankhuu, G., and P. Gomboluudev, 1996: Some characteristics of the temperature inversion over Mongolia. *Pap. Meteor. Hydrol.*, **18**, 41-46 (in Mongolian).
- Bader, D. C., and T. B. McKee, 1985: Effects of shear, stability and valley characteristics on the destruction of temperature inversions. *J. Climate Appl. Meteor.*, **24**, 822-832.
- Banta, R. M., L. Mahrt, D. Vickers, J. Sun, B. B. Balsley, Y. Pichugina, and J. Williams, 2007: The very stable boundary layer on nights with weak low-level jets. *J. Atmos. Sci.*, **64**, 3068-3090.
- Bradley, R. S., F. T. Keimig, and H. F. Diaz, 1992: Climatology of surface-based inversions in the North American Arctic. *J. Geophys. Res.*, **97**, 15699-15712.
- Chen, F., and J. Dudhia, 2001: Coupling an advanced land surface-hydrology model with the Penn State-NCAR MM5 modeling system. Part I: Model implementation and sensitivity. *Mon. Wea. Rev.*, **129**, 569-585.
- Colette, A., F. K. Chow, and L. S. Robert, 2003: A numerical study of inversion-layer breakup and the effects of topographic shading in idealized valleys. *J. Appl. Meteor.*, **42**, 1255-1272.
- Dudhia, J., 1989: Numerical study of convection observed during the winter monsoon experiment using a mesoscale two-dimensional model. *J. Atmos. Sci.*, **46**, 3077-3107.
- Eckman, R. M., 1998: Observations and numerical simulations of winds within a broad forested valley. *J. Appl. Meteor.*, **37**, 206-219.
- Friedl, M. A., and Coauthors, 2002: Global land cover mapping from MODIS: algorithms and early results. *Remote Sens. Environ.*, **83**, 287-302.
- Ganbat, G., and J.-J. Baik, 2015: Local circulations in and around the Ulaanbaatar, Mongolia, metropolitan area. *Meteor. Atmos. Phys.*, **127**, 393-406.
- Gerelchuluun, B., and J.-B. Ahn, 2014: Air temperature distribution over Mongolia using dynamical downscaling and statistical correction. *Int. J. Climatol.*, **34**, 2464-2476.
- Google Inc., 2013: Google Earth. <http://maps.google.com>.
- Grimmond, C. S. B., and Coauthors, 2010: The international urban energy balance models comparison project: First results from phase 1. *J. Appl. Meteor. Climatol.*, **49**, 1268-1292.
- Hong, S.-Y., Y. Noh, and J. Dudhia, 2006: A new vertical diffusion package with an explicit treatment of entrainment processes. *Mon. Wea. Rev.*, **134**, 2318-2341.
- Hu, X. M., J. W. Nielsen-Gammon, and F. Q. Zhang, 2010: Evaluation of three planetary boundary layer schemes in the WRF model. *J. Appl. Meteor. Climatol.*, **49**, 1831-1844.
- \_\_\_\_\_, P. M. Klein, and M. Xue, 2013a: Evaluation of the updated YSU planetary boundary layer scheme within WRF for wind resource and air quality assessments. *J. Geophys. Res.*, **118**, 10490-10505.
- \_\_\_\_\_, \_\_\_\_\_, \_\_\_\_\_, J. K. Lundquist, F. Q. Zhang, and Y. C. Qi, 2013b: Impact of low-level jets on the nocturnal urban heat island intensity in Oklahoma City. *J. Appl. Meteor. Climatol.*, **52**, 1779-1802.
- Jarvis, A., H. I. Reuter, A. Nelson, and E. Guevara, 2008: Hole-filled SRTM for the globe version 4. [Available online at <http://srtm.csi.cgiar.org>].
- Jung, J., B. Tsatsral, Y.-J. Kim, and K. Kawamura, 2010: Organic and inorganic aerosol compositions in Ulaanbaatar, Mongolia, during the cold winter on 2007 to 2008: Dicarboxylic acids, ketocarboxylic acids, and  $\alpha$ -dicarbonyls. *J. Geophys. Res.*, **115**, D22203, doi:10.1029/2010JD014339.
- Kain, J. S., 2004: The Kain-Fritsch convective parameterization: An update. *J. Appl. Meteor.*, **43**, 2318-2341.
- Kelly, R. D., 1988: Asymmetric removal of temperature inversions in a high mountain valley. *J. Appl. Meteor.*, **27**, 664-673.
- Lee, S.-H., and H.-D. Kim, 2008: Effects of regional warming due to urbanization on daytime local circulations in a complex basin of the Daegu metropolitan area, Korea. *J. Appl. Meteor. Climatol.*, **47**, 1427-1441.
- LeMone, M. A., M. Tewari, F. Chen, and J. Dudhia, 2014: Objectively determined fair-weather CBL depths in the ARW-WRF model and their comparison to CASES-97 observations. *Mon. Wea. Rev.*, **141**, 30-54.
- Li, X., X. Xia, Y. Xin, Y. Ma, J. Yang, J. Li, and X. Yang, 2012: An examination of boundary layer structure under the influence of the gap winds in Urumqi, China, during air pollution episode in winter. *J. Air. Waste Manage. Assoc.*, **62**, 26-37.
- Lin, Y. L., R. D. Farley, and H. D. Orville, 1983: Bulk parameterization of the snow field in a cloud model. *J. Climatol. Appl. Meteor.*, **22**, 1065-1092.
- Mahrt, L., and D. Vickers, 2006: Contrasting vertical structures of nocturnal boundary layers. *Bound.-Layer Meteor.*, **105**, 351-365.
- Malek, E., T. Davis, R. S. Martin, and P. J. Silva, 2006: Meteorological and environmental aspects of one of the worst national air pollution episodes (January, 2004) in Logan, Cache Valley, Utah, USA. *Atmos. Res.*, **79**, 108-122.
- Mlawer, E. J., S. J. Taubman, P. D. Brown, M. J. Iacono, and S. A. Clough, 1997: Radiative transfer for inhomogeneous atmospheres: RRTM, a validated correlated-k model for the longwave. *J. Geophys. Res.*, **102**,

- 16663-16682.
- Olofson, K. F. G., P. U. Andersson, M. Hallquist, E. Ljungström, L. Tang, D. Chen, and J. B. C. Pettersson, 2009: Urban aerosol evolution and particle formation during wintertime temperature inversions. *Atmos. Environ.*, **43**, 340-346.
- Palffy, E., 1995: Temperature inversion in the Csik basin. *Acta Climatol.*, **28-29**, 41-45.
- Ryu, Y.-H., and J.-J. Baik, 2013: Daytime local circulations and their interactions in the Seoul metropolitan area. *J. Appl. Meteor. Climatol.*, **52**, 784-801.
- \_\_\_\_\_, \_\_\_\_, and S.-H. Lee, 2011: A new single-layer urban canopy model for use in mesoscale atmospheric models. *J. Appl. Meteor. Climatol.*, **50**, 1773-1794.
- Skamarock, W. C., J. B. Klemp, J. Dudhia, D. O. Gill, D. M. Barker, M. G. Duda, X. Y. Huang, W. Wang, and J. G. Powers, 2008: A description of the advanced research WRF version 3. NCAR, Boulder, 101 pp.
- Whiteman, C. D., 1982: Breakup of temperature inversions in deep mountain valleys: Part I. Observations. *J. Appl. Meteor.*, **21**, 270-289.
- \_\_\_\_\_, and T. B. McKee, 1977: Observations of vertical atmospheric structure in a deep mountain valley. *Arch. Met. Geophys. Biokl. Ser. A.*, **26**, 39-50.
- \_\_\_\_\_, and J. C. Doran, 1993: The relationship between overlying synoptic-scale flows and winds within a valley. *J. Appl. Meteor.*, **32**, 1669-1982.
- \_\_\_\_\_, X. Bian, and S. Zhong, 1999: Wintertime evolution of the temperature inversion in the Colorado plateau basin. *J. Appl. Meteor.*, **38**, 1103-1117.